Radiotherapy and Oncology 122 (2017) 236–241

Contents lists available at ScienceDirect

Radiotherapy and Oncology

journal homepage: www.thegreenjournal.com

Head and neck radiotherapy

Dose painting by numbers based on retrospectively determined recurrence probabilities

Eric Grönlund [a,*], Silvia Johansson [b,c], Anders Montelius [a,c], Anders Ahnesjö [a,c]

[a] Medical Radiation Sciences; [b] Experimental and Clinical Oncology, Department of Immunology, Genetics and Pathology, Uppsala University; and [c] Uppsala University Hospital, Sweden

ARTICLE INFO

Article history:
Received 29 February 2016
Received in revised form 1 September 2016
Accepted 11 September 2016
Available online 1 October 2016

Keywords:
Dose painting
Dose painting by numbers
Dose painting optimization
Head and neck cancer
FDG-PET/CT

ABSTRACT

Background and purpose: The aim of this study is to derive "dose painting by numbers" prescriptions from retrospectively observed recurrence volumes in a patient group treated with conventional radiotherapy for head and neck squamous cell carcinoma.

Materials and methods: The spatial relation between retrospectively observed recurrence volumes and pre-treatment standardized uptake values (SUV) from fluorodeoxyglucose positron emission tomography (FDG-PET) imaging was determined. Based on this information we derived SUV driven dose–response functions and used these to optimize ideal dose redistributions under the constraint of equal average dose to the tumor volumes as for a conventional treatment. The response functions were also implemented into a treatment planning system for realistic dose optimization.

Results: The calculated tumor control probabilities (TCP) increased between 0.1–14.6% by the ideal dose redistributions for all included patients, where patients with larger and more heterogeneous tumors got greater increases than smaller and more homogeneous tumors.

Conclusions: Dose painting prescriptions can be derived from retrospectively observed recurrence volumes spatial relation to pre-treatment FDG-PET image data. The ideal dose redistributions could significantly increase the TCP for patients with large tumor volumes and large spread in SUV from FDG-PET. The results yield a basis for prospective studies to determine the clinical value for dose painting of head and neck squamous cell carcinomas.

© 2016 The Authors. Published by Elsevier Ireland Ltd. Radiotherapy and Oncology 122 (2017) 236–241
This is an open access article under the CC BY-NC-ND license (http://creativecommons.org/licenses/by-nc-nd/4.0/).

The radiotherapy concept "dose painting" [1] illustrates that the dose prescription for a tumor volume could be differentiated by functional imaging methods that map different dose–response levels. From this concept, the term "dose painting by numbers" [2] has evolved to distinguish that the dose prescription can be done on a voxel level. However, detailed knowledge of how image values relate to dose responses is largely lacking. Simple dose prescription functions have been proposed, such as linear relations within suitable dose ranges [3–13]. Other studies have taken a more mechanistic approach to determine dose painting prescriptions. As an example, Thorwarth et al. [14] modified the linear quadratic model with a hypoxia related parameter to determine spatially varying dose escalation factors as a basis for dose planning. By analyzing observed dose–response data from several studies, Jeong et al. [15] concluded that tumors in the head and neck region with a high uptake of fluorodeoxyglucose (FDG) likely require 10–30% more dose to reach the same control probability as tumors with a lower FDG uptake. Conclusively, it was stressed in a review by Bentzen and Grégoire [16], that the dose painting prescription ideally should be based on observed dose–response data for different functional imaging methods. Such an observation driven approach has been presented by Vogelius et al. [17], which retrospectively analyzed a group of patients treated for head and neck squamous cell carcinoma. Based on observed failure patterns, they derived dose–response functions for different contours that were distinguished by means of pre-treatment FDG-PET/CT. They used these contour driven dose–response functions in a dose optimization process to maximize the patient's tumor control probabilities (TCP) under the constraint of maintaining the average dose as compared to a conventional treatment. However, their approach did not take into consideration the dose–volume effect, i.e. how differences in tumor volume would affect the patient's expected TCP.

In this study we present an observation driven approach for "dose painting by numbers" based on retrospectively analyzed treatment data. Our dose painting approach is, in the same manner

* Corresponding author at: Sjukhusfysik ingång 82, Akademiska sjukhuset, SE-75185 Uppsala, Sweden.
E-mail address: eric.gronlund@igp.uu.se (E. Grönlund).

http://dx.doi.org/10.1016/j.radonc.2016.09.007
0167-8140/© 2016 The Authors. Published by Elsevier Ireland Ltd.
This is an open access article under the CC BY-NC-ND license (http://creativecommons.org/licenses/by-nc-nd/4.0/).

as Vogelius et al. [17], based on the assumption that image data do not directly correlate to a dose prescription, but rather to a dose–response function. We demonstrate how dose–response functions on a voxel level can be derived and how these can be used for dose painting optimization to yield dose prescriptions. We also study the potential gain in TCP by calculating ideal dose redistributions and lastly we demonstrate the use of the dose–response functions in a treatment planning system to optimize realistic dose redistributions.

Materials and methods

We start this chapter with a summary of the patient cohort used as a learning set to determine dose–response data, followed by a description of the involved mathematical procedures. We end by giving examples of how the derived dose–response data can be implemented for dose optimization.

Patient cohort data

This study is a retrospective study based on 150 consecutive patients treated between 2009 and 2014 at the Uppsala University hospital with radiotherapy (RT) for head and neck squamous cell carcinoma. The inclusion criteria were availability of pre-treatment FDG-PET/CT imaging in treatment position, and at least 6 months of follow-up. In total 59 patients met these criteria. The median follow up time was 19.3 months (range 6.3–65.6 months) after the last day of RT. All these 59 patients had completed RT with a dose to the primary clinical target volume (CTVT) between 66 and 74.5 Gy EQD_2, as determined from the fractionation patterns with $\alpha/\beta = 10$. Averaged over all treated patients this yielded a mean dose of $D_{avg} = 70.1$ Gy for 35 fractions to the CTVT volumes. In the Supplementary material we provide more information about the CTVT volumes and their SUV distributions. In total 23 of the 59 patients relapsed after RT of which 17 had a local recurrence within their CTVT. The median time to a local recurrence was 4.1 months (range 1.3–11.8 months). Out of the 17 locally relapsing patients 5 also relapsed in a lymph node region, while 6 relapsed in a lymph node region only. The median follow up time for the 42 patients that demonstrated local control was 24.9 months (range 7.2–65.6 months). Hence, the observed local tumor control frequency at D_{avg} is $TCP_{obs} = (59-17)/59 = 71.2\%$. To parameterize the patient cohorts (pc) tumor control probability, a logistic function [18] was chosen such that

$$TCP_{pc}(D) = \frac{1}{1 + \left(\frac{D_{50,pc}}{D}\right)^{4\gamma_{50,pc}}}, \tag{1}$$

with $\gamma_{50,pc} = 1.8$ taken from the literature [19], and $D_{50,pc} = 61.9$ Gy determined so that TCP_{pc} at $D = D_{avg}$ equal the observed TCP_{obs}.

Delineation of recurrent tumor volumes

All 17 local recurrences were confirmed by biopsies. The recurrence volumes (RVs) were manually delineated on the CT slices from the pre-treatment PET/CT by an experienced radiation oncologist. To avoid biasing the delineation, none of the pre-treatment PET images or originally delineated CTVT volumes were shown during this process. The delineation process was supported by informed consent using post-treatment images and follow up data, such as physical examination of the patients and pathological statements from biopsies. Available post-treatment images were shown on a screen next to the one where the delineation was done. All 17 patients had a post-treatment CT of which 13 also had a post-treatment PET/CT. Out of these 13 patients, 7 also had a post-treatment MRI examination. The dose painting robustness with regard to the RV delineations was tested through use of two additional sets of RVs that were decreased or expanded from the delineated RVs. The decreased volumes were derived by creating new contours with a patient specific uniform distance from the delineated contours such that the RVs were reduced to 50% of its original volume. These decreased contours were all within a uniform distance of 1.0–2.5 mm from the delineated contours. The expanded volumes were constructed by adding a margin of 3.3 mm, which corresponds to the 95 percentile of a normal distribution with a standard deviation of 2 mm, assumed to be a reasonable contouring distance uncertainty. In both cases, the new contours were created by using 3D distance maps based on the original contours.

Derivation of SUV driven dose–response functions

We will now derive dose–response functions dependent on absolute SUV in voxels, but this derivation formalism could also be applied for relative image data normalized to e.g. the maximum SUV for a patient. To model a dose–response function in principle any parameterizable sigmoidal function can be used, but we adopt the logistic function with the logarithm of dose as covariate [18]. This function is often used for statistical applications and we adopt it because it forces the probability to zero when the dose goes to zero, thus allowing a realistic behavior for large dose ranges. The SUV specific dose–response functions to be determined will hence be described by

$$TCP_{vox}(D, SUV) = \frac{1}{1 + \left(\frac{D_{50}(SUV)}{D}\right)^{4\gamma_{50,eff}}}, \tag{2}$$

where $D_{50}(SUV)$ is assigned to be a function of SUV and $\gamma_{50,eff}$ is set to be constant as in Vogelius et al. [17]. In the following, we show how to determine $D_{50}(SUV)$ and $\gamma_{50,eff}$ from voxel based recurrence frequencies using the simplification that every CTVT voxel for all included patients has received an equal dose of D_{avg} (we will later slightly relax this condition). From the 17 delineated RVs and the 59 treated CTVTs, we determine the SUV frequency distribution $f_{RVs}(SUV)$ for the RVs and the SUV frequency distribution $f_{(RVs \cup CTVTs)}(SUV)$ for the union of all RVs and CTVTs. From these we define a local control ratio (LCR) as a function of SUV

$$LCR(SUV) = 1 - \frac{f_{RVs}(SUV)}{f_{(RVs \cup CTVTs)}(SUV)}. \tag{3}$$

To transform this LCR function into SUV dependent voxel specific TCP_{vox} values we introduce a normalizing exponent k that takes into account the used dose voxel sizes and also reconstructs the observed tumor control TCP_{obs} for the population. Under the assumption of voxel independency, the TCP for a volume is calculated by multiplying the individual TCP_{vox} values belonging to the volume. Hence, k is determined such that

$$TCP_{vox}(D_{avg}, SUV) = (LCR(SUV))^k, \tag{4}$$

and

$$TCP_{obs}(D_{avg}) = \frac{1}{N}\sum_{pat}\prod_{vox \in CTVT_{pat}} TCP_{vox}(D_{avg}, SUV) \tag{5}$$

are fulfilled, where Eq. (4) preserves the calculated LCR, and Eq. (5) imposes that the average resulting TCP over all N patients equals the observed tumor control within the patient cohort. It follows that k will be inversely proportional to the dose voxel volume since smaller voxels imply more multiplications needing higher TCP_{vox} values to preserve TCP_{obs} and the LCR values. With k determined from Eqs. (4) and (5), we have TCP_{vox} values for all SUV determined at D_{avg}, but not for other dose values. In order to achieve a general

$\mathrm{TCP}_{\mathrm{vox}} = \mathrm{TCP}_{\mathrm{vox}}(D, \mathrm{SUV})$ relation based on Eq. (2) so that we can calculate each patient's resulting TCP value

$$\mathrm{TCP}_{\mathrm{pat}}(D) = \prod_{\mathrm{vox}\in\mathrm{CTVT}_{\mathrm{pat}}} \frac{1}{1+\left(\frac{D_{50}(\mathrm{SUV})}{D}\right)^{4\gamma_{50,\mathrm{eff}}}}, \tag{6}$$

the unknowns $D_{50}(\mathrm{SUV})$ and $\gamma_{50,\mathrm{eff}}$ must be determined. To do so, we first solve $D_{50}(\mathrm{SUV})$ from Eqs. (2) and (4) to get

$$D_{50}(\mathrm{SUV}) = D_{\mathrm{avg}} \cdot \left(\frac{1}{(\mathrm{LCR}(\mathrm{SUV}))^{k}} - 1\right)^{\frac{1}{4\gamma_{50,\mathrm{eff}}}}, \tag{7}$$

which contains the yet unknown $\gamma_{50,\mathrm{eff}}$. We now introduce the requirement that at D_{avg} the dose derivative of Eq. (6) averaged over all N patients should equal the dose derivative of Eq. (1) for the patient cohort, i.e.

$$\frac{1}{N}\sum_{\mathrm{pat}} \frac{\mathrm{d}(\mathrm{TCP}_{\mathrm{pat}}(D))}{\mathrm{d}D}\bigg|_{D=D_{\mathrm{avg}}} = \frac{\mathrm{d}(\mathrm{TCP}_{\mathrm{pc}}(D))}{\mathrm{d}D}\bigg|_{D=D_{\mathrm{avg}}}, \tag{8}$$

which enables us to solve for $\gamma_{50,\mathrm{eff}}$. To show that, we apply the derivative identity

$$\frac{\mathrm{d}(\mathrm{TCP}_{\mathrm{pat}}(D))}{\mathrm{d}D} = \mathrm{TCP}_{\mathrm{pat}}(D) \sum_{\mathrm{vox}\in\mathrm{CTVT}_{\mathrm{pat}}} \frac{\frac{\mathrm{d}(\mathrm{TCP}_{\mathrm{vox}}(D))}{\mathrm{d}D}}{\mathrm{TCP}_{\mathrm{vox}}(D)}, \tag{9}$$

on Eq. (6), and by use of Eqs. (2) and (7) we get

$$\frac{\frac{\mathrm{d}(\mathrm{TCP}_{\mathrm{vox}}(D))}{\mathrm{d}D}}{\mathrm{TCP}_{\mathrm{vox}}(D)}\bigg|_{D=D_{\mathrm{avg}}} = \gamma_{50,\mathrm{eff}} \frac{4(1-(\mathrm{LCR}(\mathrm{SUV}))^{k})}{D_{\mathrm{avg}}}, \tag{10}$$

from which $\gamma_{50,\mathrm{eff}}$ can be solved by combining Eqs. (1), (8) and (10) yielding

$$\gamma_{50,\mathrm{eff}} = \gamma_{50,\mathrm{pc}} \frac{(D_{50,\mathrm{pc}}/D_{\mathrm{avg}})^{4\gamma_{50,\mathrm{pc}}}}{\left(1+(D_{50,\mathrm{pc}}/D_{\mathrm{avg}})^{4\gamma_{50,\mathrm{pc}}}\right)^{2}} \cdot \frac{N}{\sum_{\mathrm{pat}}\mathrm{TCP}_{\mathrm{pat}}(D_{\mathrm{avg}})\sum_{\mathrm{vox}\in\mathrm{CTVT}_{\mathrm{pat}}}(1-(\mathrm{LCR}(\mathrm{SUV}))^{k})}. \tag{11}$$

With $\gamma_{50,\mathrm{eff}}$ known, $D_{50}(\mathrm{SUV})$ can be determined for all SUV by inserting $\gamma_{50,\mathrm{eff}}$ into Eq. (7). While doing that, D_{avg} can be substituted with a more accurate dose estimate for different SUV to reduce the effect of introducing an average D_{avg} in the first place. Finally, with all needed components for Eq. (2) known, we can use Eq. (2) for dose painting optimization.

Dose painting optimization

As in Vogelius et al. [17], we choose to find optimal dose redistributions requiring that the average dose $\bar{D}$ for the target volumes is kept equal to D_{avg}. Hence, we use the SUV driven dose–response functions to optimize the dose per voxel $D = D(\mathrm{vox})$ with the objective to maximize a patient's tumor control probability

$$\begin{aligned} &\underset{D}{\text{maximize}} \quad \prod_{\mathrm{vox}\in\mathrm{CTVT}_{\mathrm{pat}}} \mathrm{TCP}_{\mathrm{vox}}(D, \mathrm{SUV}) \\ &\text{subject to} \quad \bar{D} = D_{\mathrm{avg}} \end{aligned}. \tag{12}$$

Firstly, we want to find ideal dose redistributions not constrained by radiation transport phenomena causing dose correlations with nearby voxels. Such ideal dose redistributions were solved numerically by use of the FindMaximum function in Mathematica® (Wolfram Research, Inc., Mathematica, v. 10.0, Champaign, IL (2014)). Secondly, we relax this constraint to demonstrate a dose painting example under more realistic conditions by implementing Eq. (12) into a research version of a treatment planning system (RayStation® v. 4.6.100.10, RaySearch Laboratories AB, Stockholm).

Results

The voxel sizes for the retrospective patient data were $1.95 \times 1.95 \times 3.27\ \mathrm{mm}^3$ for the SUV grid and $3.00 \times 3.00 \times 2.50\ \mathrm{mm}^3$ for the dose grid. We chose to base the entire analysis on the used dose grid voxel size and hence the SUV voxels were resampled by trilinear interpolation to fit the dose grid. The LCR values were determined according to Eq. (3) for the different RV delineation scenarios based on a discretization of SUV into bins of width 1 SUV. The LCR functions decreased with increasing SUV except for the highest observed SUV, as shown in Fig. 1. However, with increasing SUV the number of voxels were strongly decreasing and hence diminishing the significance of the LCR values at higher SUV. To circumvent this, we used a weighted linear fit for each delineation scenario with the frequency of respective SUV as weights, shown in Fig. 1. The exponent k, solved according to Eqs. (4) and (5) for the linearized LCR functions, equaled 0.00497, 0.00277 and 0.00144 for the decreased, delineated and expanded RVs.

Fig. 2 shows the calculated D_{50} functions according to Eq. (7) for the linearized LCR functions corresponding to the different delineation scenarios. These are very similar to each other in spite of the different LCR functions shown in (Fig. 1 Right), which is a consequence of reconstructing the populations $\mathrm{TCP}_{\mathrm{obs}}$ with the exponent k. From the D_{50} functions it is evident that the SUV driven

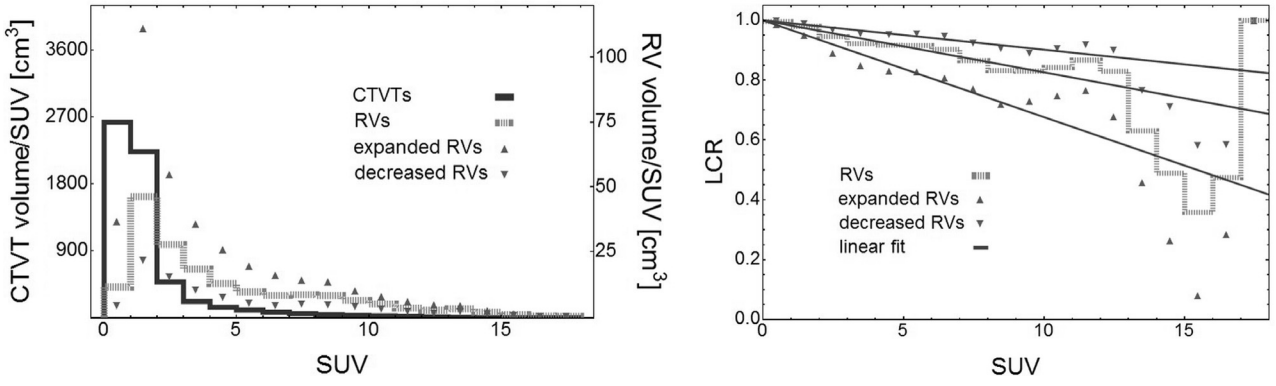

Fig. 1. (Left) Frequency distributions of SUV for all 59 CTVTs and for the 17 delineated, expanded and decreased RVs. (Right) LCR calculated according to Eq. (3) for the delineated, expanded and decreased RVs. Also shown are the linearized LCR functions, calculated by a weighted linear fit for each delineation scenario. The weighting function equals the sum of the CTVT and RV distributions shown to the left.

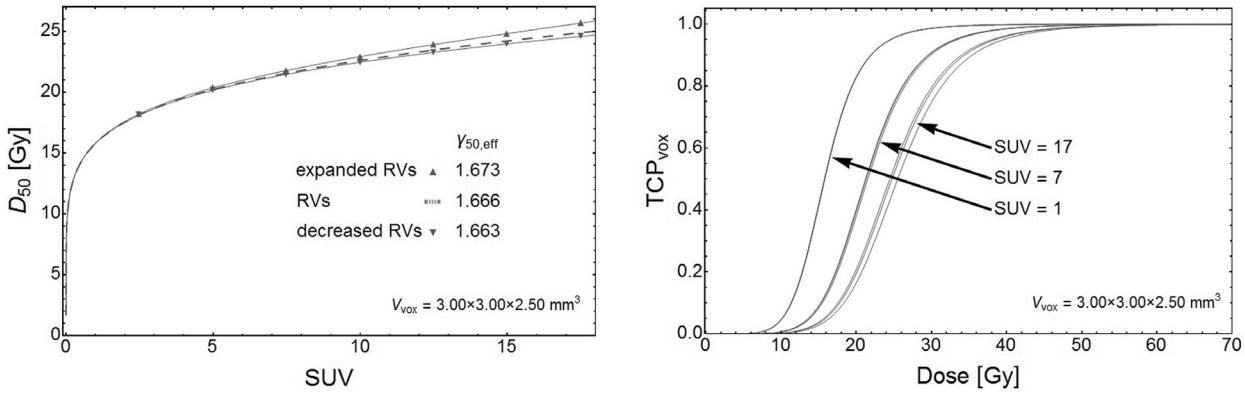

Fig. 2. (Left) D_{50} as a function of SUV and the determined $\gamma_{50,eff}$ values solved for the linearized LCR functions for the different delineation scenarios. (Right) SUV driven dose–response functions for the different delineation scenarios for three different SUV. At SUV = 1 and SUV = 7 are the functions for the different delineation scenarios not distinguishable from each other, while for at SUV = 17 a slight separation is observed with the expanded RVs rightmost and the decreased RVs leftmost.

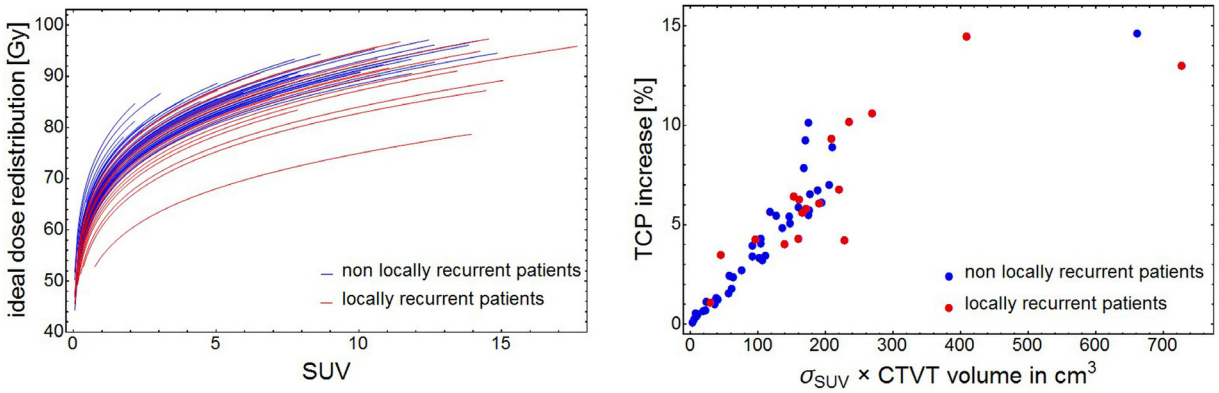

Fig. 3. (Left) The 59 patient's ideal dose redistributions dependent on SUV within their CTVTs. (Right) Each patient's increase in TCP by the ideal dose redistributions compared to a homogenous dose distribution, dependent on the standard deviation of SUV multiplied by the CTVT volumes.

dose–response functions, as shown in Fig. 2, demonstrates an increasing radio resistance with increasing SUV.

By optimizing according to Eq. (12), each patient received an ideal dose redistribution as shown in Fig. 3. The individual TCP increases compared to a standard treatment with a homogeneous dose of D_{avg} were ranging between 0.1% and 14.6%, as visualized dependent on the standard deviation of SUV multiplied by the CTVT volume in Fig. 3. Clearly, the potential to increase the TCP for a patient with dose painting increases with higher SUV heterogeneity and larger CTVT volumes. The locally recurrent patients had in general a higher TCP increase than the locally controlled patients, and the locally recurrent patient with the highest TCP increase went from 45.3% to 59.8%. The lowest TCP increase of 0.1% was observed for a locally controlled patient, with a TCP of 96.0% for a homogeneous dose distribution. The average increase was 4.9% for the whole patient group, meaning that if all patients were treated with their corresponding ideal dose redistribution, the patient cohorts observed TCP_{obs} = 71.2% would raise to 71.2 + 4.9 = 76.1%. As expected by the very similar D_{50} functions from the decreased and expanded RVs, the corresponding average TCP increases were 76.0% and 76.3%.

To include realistic radiation transport phenomena into the optimization, the objectives and constraints described by Eq. (12) were implemented into RayStation, and a more realistic dose optimization was performed for a patient that had an ideal dose redistribution very similar to the median of all the ideal dose redistributions. The realistic dose optimization was done by planning with 6 MV and volumetric modulated arc therapy (VMAT) with 2 arcs completing a full rotation and letting the optimizer iterate until an optimal solution was found. The resulting realistic dose redistribution is demonstrated in Fig. 4, where also for comparison this patient's ideal dose is shown. For a homogeneous dose distribution of D_{avg}, the expected TCP for this patient was 60.1%. The planned realistic dose redistribution resulted in a TCP of 66.3% compared to the TCP of 67.0% using the ideal dose redistribution.

Discussion

This study presents an observation driven approach for "dose painting by numbers" that demonstrates how dose–response functions for pre-treatment image data can be derived based on post-treatment recurrences. There are no underlying mechanistic assumptions in the method, it is simply based on assumed sigmoidal dose–response curves and image data observed to correlate to recurrence locations. It is hence likely that the approach is not limited to FDG-PET imaging, but could be applied for other imaging methods where image data can be correlated to a spatial variation in TCP. The derived dose–response functions are in our case, however, only valid for voxels within the CTVT volumes. To prescribe dose for lymph node regions, the key problem is to determine the spatially varying risk for spread, not the spatially varying risk

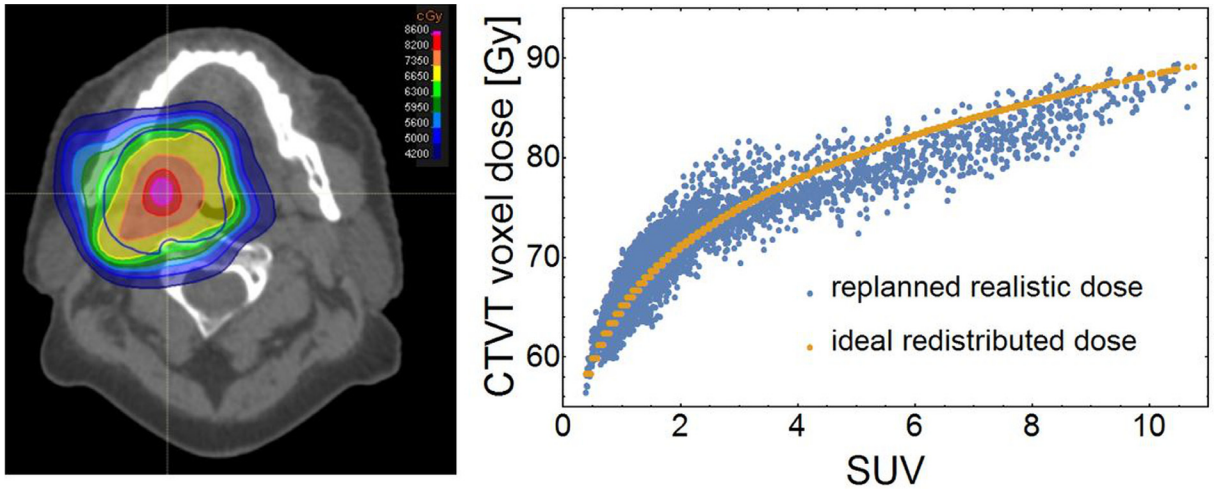

Fig. 4. (Left) The objective function described by Eq. (12) used for realistic dose redistribution in RayStation for one of the patient's CTVT. (Right) The realistic dose redistribution in relation to SUV for this patient and for comparison this patient's ideal dose redistribution.

for a local recurrence. Therefore, we concluded that the lymph node relapses were outside the scope of this study.

The resolution of PET is limited by partial volume effects [20] and the cameras technical abilities. Resolution issues for PET imaging were demonstrated by Christian et al. [21] who analyzed differences between PET images and high resolution autoradiography images. However, the physical limitations due to clinical dose delivery processes result in dose distributions with a limited resolution, likely with an order of magnitude not too different from the clinical PET resolution. Due et al. [22] observed a correlation between FDG-uptake and recurrence locations. Our dose painting approach is based on our own similar observations, without making assumptions about unresolved patterns of FDG-uptake. Another limitation lies in the manual drawing of recurrence volumes on the pre-treatment CT images that affect which SUV regions are considered to be recurrent. To test this, we decreased and expanded the delineated RVs and calculated corresponding LCR functions as shown in Fig. 1. By deriving dose–response functions from these LCR functions and optimizing according to Eq. (12), it was noticed that the TCP increases for the whole population only differed by a maximum of 0.2%. This robustness with regard to the delineations is a result of the requirements imposed by Eqs. (4) and (5) to maintain the observed $TCP_{obs} = 71.2\%$ for all LCR functions that resulted in different normalizing exponents k.

The ideal dose redistributions shown in Fig. 3, are based on the constraint of a mean dose of $D_{avg} = 70.1$ Gy to the CTVT for each patient. It was observed that the maximum and minimum dose levels were varying between patients. This is explained by that a patient with a high median SUV has less dose to spend on the high SUV voxels, while a patient with a low median SUV can spend more dose on these voxels. A consequence is that the use of relative SUV instead of absolute would yield similar dose distributions. This was confirmed by redoing the full procedure based on relative SUV data, although with the interest of space we chose to not present these results. For all patients, the ideal dose redistributions increased the calculated TCP compared to a homogeneous dose, but not all showed a significant increase. Based on the presented dose painting approach would patients with larger tumor volumes and greater SUV heterogeneity gain more from dose painting, which potentially could be used as an indicator for patient selection.

Regarding the dose–volume effect, Vogelius et al. [17] implicitly assumed that all patient's TCP values are the same for a homogeneous dose distribution and independent of any differences in tumor volume. In this study a dose–volume effect is introduced since the TCP calculation for a patient according to Eq. (6) is performed by each patient's specific number of CTVT voxels. The TCP product models the dose–volume effect, which also is the case in the TCP modeling presented by Ebert and Hoban [23] that also assumed that voxels are controlled independently of each other.

The presented dose optimization yielded dose levels that exceed what is reported as a maximum tolerated dose of 86 Gy for 35 fractions [7,10,24]. However, since the high SUV subvolumes are relatively small, the relative gain in TCP for the whole patient group decreases only by 0.1% by adding a maximum dose constraint of 86 Gy. Dose constraints or normal tissue complication probability (NTCP) requirements are necessary to avoid exceedingly high doses when using dose–response functions for optimization. It is likely that other constraints are more relevant from a medical perspective, but elaborating on these is outside the scope of this paper.

Prospective clinical trials are needed to confirm that the presented framework for derivation of dose–response functions can yield the indicated improvements. For example, the study from Trani et al. [25] indicates that dose painting does not improve tumor control for rats. In our study we did not take into consideration adaptive approaches with dose prescriptions updated by imaging between treatment fractions. However, the study from Berwouts et al. [9] has shown the feasibility for adaptive FDG driven dose painting, and Rasmussen et al. [26] reported that pre-treatment FDG-PET/CT gives a stable spatio-temporal basis for dose painting of head and neck squamous cell carcinomas. A possible complication for adaptive FDG driven dose painting can be false positive FDG uptake caused by inflammatory reactions of irradiated tissues.

Conclusions

In this study, we have shown that dose painting prescriptions from FDG-PET images potentially can be used to improve treatment results for head and neck squamous cell carcinomas. The possible increases in tumor control probability compared to a conventional treatment varied from 0.1% to 14.6% where the improvements were greater for patients with large tumor volumes and large spread in SUV. Based on our results, prospective clinical trials could be planned to determine the clinical value and potential for dose painting of head and neck squamous cell carcinomas.

Conflict of interest statement

We declare no conflict of interest.

Acknowledgements

This research was supported by the Swedish Cancer Society, grant number 130632. We are grateful to Erik Traneus at RaySearch Laboratories AB, for helping out with the implementation of a dose painting objective function.

Appendix A. Supplementary data

Supplementary data associated with this article can be found, in the online version, at http://dx.doi.org/10.1016/j.radonc.2016.09.007.

References

[1] Ling CC, Humm J, Larson S, Amols H, Fuks Z, Leibel S, et al. Towards multidimensional radiotherapy (MD-CRT): biological imaging and biological conformality. Int J Radiat Oncol Biol Phys 2000;47:551–60.
[2] Bentzen SM. Theragnostic imaging for radiation oncology: dose-painting by numbers. Lancet Oncol 2005;6:112–7.
[3] Alber M, Paulsen F, Eschmann SM, Machulla HJ. On biologically conformal boost dose optimization. Phys Med Biol 2003;48:N31.
[4] Das SK, Miften MM, Zhou S, Bell M, Munley MT, Whiddon CS, et al. Feasibility of optimizing the dose distribution in lung tumors using fluorine-18-fluorodeoxyglucose positron emission tomography and single photon emission computed tomography guided dose prescriptions. Med Phys 2004;31:1452. http://dx.doi.org/10.1118/1.1750991.
[5] Vanderstraeten B, Duthoy W, Gersem WD, Neve WD, Thierens H. [18F]fluoro-deoxy-glucose positron emission tomography ([18F]FDG-PET) voxel intensity-based intensity-modulated radiation therapy (IMRT) for head and neck cancer. Radiother Oncol 2006;79:249–58. http://dx.doi.org/10.1016/j.radonc.2006.03.003.
[6] Rickhey M, Koelbl O, Eilles C, Bogner L. A biologically adapted dose-escalation approach, demonstrated for 18F-FET-PET in brain tumors. Strahlenther Onkol 2008;184:536–42. http://dx.doi.org/10.1007/s00066-008-1883-6.
[7] Duprez F, De Neve W, De Gersem W, Coghe M, Madani I. Adaptive dose painting by numbers for head-and-neck cancer. Int J Radiat Oncol 2011;80:1045–55. http://dx.doi.org/10.1016/j.ijrobp.2010.03.028.
[8] Witte M, Shakirin G, Houweling A, Peulen H, van Herk M. Dealing with geometric uncertainties in dose painting by numbers: introducing the ΔVH1. Radiother Oncol 2011;100:402–6. http://dx.doi.org/10.1016/j.radonc.2011.08.028.
[9] Berwouts D, Olteanu LAM, Duprez F, Vercauteren T, De Gersem W, De Neve W, et al. Three-phase adaptive dose-painting-by-numbers for head-and-neck cancer: initial results of the phase I clinical trial. Radiother Oncol 2013;107:310–6. http://dx.doi.org/10.1016/j.radonc.2013.04.002.
[10] Differding S, Sterpin E, Janssens G, Hanin F-X, Lee JA, Grégoire V. Methodology for adaptive and robust FDG-PET escalated dose painting by numbers in head and neck tumors. Acta Oncol 2015:1–9. http://dx.doi.org/10.3109/0284186X.2015.1046997.
[11] Arnesen MR, Knudtsen IS, Rekstad BL, Eilertsen K, Dale E, Bruheim K, et al. Dose painting by numbers in a standard treatment planning system using inverted dose prescription maps. Acta Oncol 2015;54:1607–13. http://dx.doi.org/10.3109/0284186X.2015.1061690.
[12] Fontanarosa D, Witte M, Meijer G, Shakirin G, Steenhuijsen J, Schuring D, et al. Probabilistic evaluation of target dose deterioration in dose painting by numbers for stage II/III lung cancer. Pract Radiat Oncol 2015.
[13] Barragán AM, Differding S, Janssens G, Lee JA, Sterpin E. Feasibility and robustness of dose painting by numbers in proton therapy with contour-driven plan optimization. Med Phys 2015;42:2006–17. http://dx.doi.org/10.1118/1.4915082.
[14] Thorwarth D, Eschmann S-M, Paulsen F, Alber M. Hypoxia dose painting by numbers: a planning study. Int J Radiat Oncol 2007;68:291–300. http://dx.doi.org/10.1016/j.ijrobp.2006.11.061.
[15] Jeong J, Setton JS, Lee NY, Oh JH, Deasy JO. Estimate of the impact of FDG-avidity on the dose required for head and neck radiotherapy local control. Radiother Oncol 2014;111:340–7. http://dx.doi.org/10.1016/j.radonc.2014.03.018.
[16] Bentzen SM, Gregoire V. Molecular imaging-based dose painting: a novel paradigm for radiation therapy prescription. Semin Radiat Oncol 2011;21:101–10. http://dx.doi.org/10.1016/j.semradonc.2010.10.001.
[17] Vogelius IR, Håkansson K, Due AK, Aznar MC, Berthelsen AK, Kristensen CA, et al. Failure-probability driven dose painting. Med Phys 2013;40:81717. http://dx.doi.org/10.1118/1.4816308.
[18] Bentzen SM, Tucker SL. Quantifying the position and steepness of radiation dose-response curves. Int J Radiat Biol 1997;71:531–42. http://dx.doi.org/10.1080/095530097143860.
[19] Bentzen SM. Radiobiological considerations in the design of clinical trials. Radiother Oncol 1994;32:1–11.
[20] Soret M, Bacharach SL, Buvat I. Partial-volume effect in PET tumor imaging. J Nucl Med 2007;48:932–45.
[21] Christian N, Lee JA, Bol A, De Bast M, Jordan B, Grégoire V. The limitation of PET imaging for biological adaptive-IMRT assessed in animal models. Radiother Oncol 2009;91:101–6. http://dx.doi.org/10.1016/j.radonc.2008.11.014.
[22] Due AK, Vogelius IR, Aznar MC, Bentzen SM, Berthelsen AK, Korreman SS, et al. Recurrences after intensity modulated radiotherapy for head and neck squamous cell carcinoma more likely to originate from regions with high baseline [18F]-FDG uptake. Radiother Oncol 2014;111:360–5. http://dx.doi.org/10.1016/j.radonc.2014.06.001.
[23] Ebert MA, Hoban PW. Some characteristics of tumour control probability for heterogeneous tumours. Phys Med Biol 1996;41:2125. http://dx.doi.org/10.1088/0031-9155/41/10/019.
[24] Madani I, Duprez F, Boterberg T, Van de Wiele C, Bonte K, Deron P, et al. Maximum tolerated dose in a phase I trial on adaptive dose painting by numbers for head and neck cancer. Radiother Oncol 2011;101:351–5. http://dx.doi.org/10.1016/j.radonc.2011.06.020.
[25] Trani D, Yaromina A, Dubois LJ, Granzier M, Peeters SG, Biemans R, et al. Preclinical assessment of efficacy of radiation dose painting based on intratumoral FDG-PET uptake. Clin Cancer Res 2015. clincanres–0290.
[26] Rasmussen JH, Vogelius IR, Aznar MC, Fischer BM, Christensen CB, Friborg J, et al. Spatio-temporal stability of pre-treatment 18F-Fludeoxyglucose uptake in head and neck squamous cell carcinomas sufficient for dose painting. Acta Oncol 2015;54:1416–22. http://dx.doi.org/10.3109/0284186X.2015.1061694.